Article

Rapid Screening of Retrieved Knee Prosthesis Components by Confocal Raman Micro-Spectroscopy

Calin Tudor Hozan [1], Simona Cavalu [2],*, Simona Cinta Pinzaru [3],*, Aurel George Mohan [1], Florin Beteg [4] and Gelu Murvai [1]

1   Faculty of Medicine and Pharmacy, Surgery Department, University of Oradea, P-ta 1Decembrie 10, 410073 Oradea, Romania; chozan@uoradea.ro (C.T.H.); mohanaurel@uoradea.ro (A.G.M.); gelu.murvai@csud.uoradea.ro (G.M.)
2   Faculty of Medicine and Pharmacy, Preclinical Sciences Department, University of Oradea, P-ta 1 Decembrie 10, 410073 Oradea, Romania
3   Biomolecular Physics Department, Babes-Bolyai University, Kogalniceanu 1, 400084 Cluj-Napoca, Romania
4   Department of Veterinary Medicine, University of Agricultural Sciences and Veterinary Medicine, Calea Manastur 3-5, 400372 Cluj-Napoca, Romania; florin.beteg@usamvcluj.ro
*   Correspondence: simona.cavalu@gmail.com (S.C.); simona.cinta@phys.ubbcluj.ro (S.C.P.)

check for updates

Featured Application: Application of confocal Raman spectroscopy in search of failure reason in knee arthroplasty.

Abstract: (1) Aim: To evaluate the failure reason and surface modifications of a retrieved knee prosthesis; (2) Methods: Rapid confocal Raman spectroscopy screening was applied on the surface of a retrieved knee prosthesis (both titanium and UHMWPE (Ultra-high-molecular-weight polyethylene) component) in order to determine predominate implant damage, along with the chemical composition of synovial fluid accumulated in the stem of the tibial component during the implantation period. Correlations between the medical records of the patient (clinical and radiographic information) and spectroscopic results are pointed out, the parameters being interpreted in the context of proper functioning and life span of knee prosthesis; (3) Results: The metallic tibial component does not show any modification during the implantation period, as demonstrated by the well preserved titanium component with signature of anatase phase detected in retrieved component, compared to unused piece. The spectral features of polymeric component (ultrahigh molecular weight polyethylene, UHMWPE) revealed structural modification in crystallinity and amorphous phase accompanied by insignificant level of oxidation (OI < 1). Scratching, pitting and persistent organic spots as a result of mechanical and chemical deterioration were noticed on the surface of retrieved insert. Acrylic cement deterioration was also noticed. Synovial fluid collected from the stem of the tibial component demonstrated a lipidomic profile; (4) Conclusions: Combining the clinical evidences with confocal Raman spectroscopy allowed a rapid screening with high sensitivity and nondestructive measurements in the case of failure in TKA (total knee arthroplasty). The third body wear and lipidomic profile of synovial fluid are cumulative factors of failure in this case, resulting in an osteolysis that finally leads to an aseptic loosening.

Keywords: knee prosthesis failure; arthroplasty; confocal raman spectroscopy

1. Introduction

The most common types of arthritis (severe degenerative joint disease) which may affect the knee joint are osteoarthritis, rheumatoid arthritis and traumatic arthritis. In osteoarthritis, the breakdown of joint

cartilage and adjacent bone may occur, affecting both middle-aged and older adults. The rheumatoid arthritis is causes by the inflammation of the synovial membrane, resulting in excess of synovial fluid, while the traumatic arthritis is due to a serious injury [1]. If medical treatments are not satisfactory, knee arthroplasty or total knee replacement (TKR) is applied, which is a surgical procedure to resurface a knee damaged by arthritis. The components of artificial knee replicate the shape of joint surface, reestablishing the smooth rolling and gliding movement. Evan if there are different models of knee implants available from a number of different manufacturers, a typical knee prosthesis is generally comprised of three components: (a) the tibial component (shin bone, metallic, stemmed, with a tibial plateau), (b) the femoral component (thigh bone, metallic) with a curved surface and a central grove mimicking the surface of femur and (c) the polyethylene insert as a load bearing and articulating surface with a corresponding curvature that accept the opposite femoral surface [2]. During knee replacement surgery, these implant components are usually connected to the bone with acrylic cement.

Usually, cases of failure in total knee replacement (TKR) are caused by wear and tear with subsequent loosening of the implant, either cemented or cementless. Other causes are infection, instability, fracture or stiffness [3,4]. Designs of total knee implants have a variety of contact geometries, in which the contact between metallic and polyethylene components articulating with each other results in a complex stress distribution pattern. The main reason for failure is the high friction coefficient of these materials that can lead to the release of wear debris from the implant into the bloodstream. As a result, an inflammation of the surrounding tissue occurs and gives rise to the bone resorption (osteolysis), which ultimately leads to loosening of the implant and hence the implant must be replaced by a new one [4]. In general, joint simulators allow preclinical evaluation of wear of artificial joints in a controlled environment [5,6]. However, it is difficult to create similar dynamic conditions as during natural movement of joints after implantation while simulating conditions. During the walking cycle, the knee joint prosthesis is subjected to cyclic loading, causing fatigue failure and sliding between insert and femoral component, which enhances the wear process in plastic insert [7]. Pre-clinical testing of components is vital to find out the probability of damage or time dependence of wear. While laboratory simulation can provide important data related to long-term mechanical performance of materials used in arthroplasty, the spectroscopic analysis of retrieved knee prosthesis components provides invaluable insights into the in vivo tribological performance of the prostheses [8]. According to previous reports [9], damage modes identified in retrieved components of knee prosthesis includes abrasion, burnishing, extruded cement, dishing, embedding, pitting and scratching [9], as demonstrated by scanning electron microscopy (SEM) micrographs. Especially plastic ultra-high-molecular-weight polyethylene (UHMWPE) component failure is known to occur through different causes: delamination, crack formation, wear, pitting and the generation of particulate debris with a local resorptive osteoclastic response [10]. Not only mechanical damage to the materials may contribute to complications requiring revision surgery, but also degradation of the articulating surfaces associated with the release of wear debris to surrounding tissues may also contribute to failure and the need for revision surgery [11]. Accumulating wear debris after total joint arthroplasty may leads to an aseptic loosening of the prosthesis, being demonstrated that the number, size and shape of the wear particles strongly influence the extent of the inflammatory biologic reaction and consequently the periprosthetic osteolysis and early failure of the prosthesis [12].

On the other hand, synovial fluid response to particulate UHMWPE has been also documented by many authors [13–17]. In some of these studies [13,17], Raman spectroscopy was used to assess the biochemical composition of synovial fluid collected from patients with clinical evidence of knee osteoarthritis or presenting a chronic inflammatory response like synovitis and it has been hypothesized that in some cases, such a synovial reaction may contribute to component loosening. Based on the carotenoids resonance Raman signal jointly exploited along the surface-enhanced Raman scattering (SERS) signal of proteins from synovial fluid, a discrimination of high- and low-grade osteoarthritis has been proposed using multivariate data analysis [17]. Several chemical changes may occur in cartilage as a result of osteoarthritis, which include the loss of proteoglycan content and collagen degradation [17].

Synovial fluid is primarily composed of water, proteins, proteoglycans, glycosaminoglycans with crucial role in joints lubrication, lipids, small inorganic salts and metabolites such as amino acids or sugars, each of these components having particular function in maintaining viscoelastic properties and regulating the biologic activity of cytokines and enzymes involved in osteoarthritis [16,17].

Here, a retrieved knee prosthesis (both titanium and UHMWPE component) after 10 years use was investigated. In addition, chemical composition of synovial fluid accumulated in the stem of the tibial component during implantation period was analyzed, aiming to determine the implant failure cause. Using confocal micro-Raman spectroscopy, the retrieved polyethylene component was compared with a newly open counterpart, to assess molecular changes associated with aging process in physiological medium. Metal–plastic aging and the possible scenario of failure due to combined effect of mechanical and biochemical processes that may affect the longevity of knee prostheses are discussed. Correlations between the medical records of the patient (clinical and radiographic information) and our spectroscopic results are proposed.

2. Materials and Methods

2.1. Clinical Case Description

The present study was performed in agreement with the ethical standards of the Helsinki Declaration and approved by the Ethical Committee of University of Oradea, Romania (ref. nr. 08/05.2020); the patient signed an informed consent agreement for the surgical protocol. The patient was a 60-year-old male, admitted to the orthopedics clinic I at the Emergency County Hospital, Oradea (Romania) claiming right knee pain and partial functional impotence of the right pelvic limb. From the personal pathologic background of the patient, we noted that he was the victim of a car crush and suffered a fracture of the right tibial plateau, eight years before medical examination, for which surgery was performed. Additionally, the patient presented hydrostatic varices of the lower limbs bilaterally, lumbar spondylosis and lumbar discopathy. After clinical and paraclinical examination (radiological exam), the diagnosis was established: right gonarthrosis which appeared secondary to a tibial plateau fracture. Total cemented arthroplasty at the level of the right knee was performed using NexGen® complete knee solution (Zimmer, Warsaw, IN, USA) and Gentafix®1 (Teknimed, Vic en Bigorre, France) acrylic bone cement. The patient had a favorable evolution after surgery. After 10 years, a clinical and radiological reassessment was made; a destabilization of the tibial component was noticed. As a consequence, revision of the total knee arthroplasty was performed. During the surgery, it the instability of the tibial components accompanied by decementation and loosening was noticed. No sign of sepsis was found. The radiological examination before and after arthroplasty and revision surgery is presented in Figure 1.


Figure 1. *Cont.*
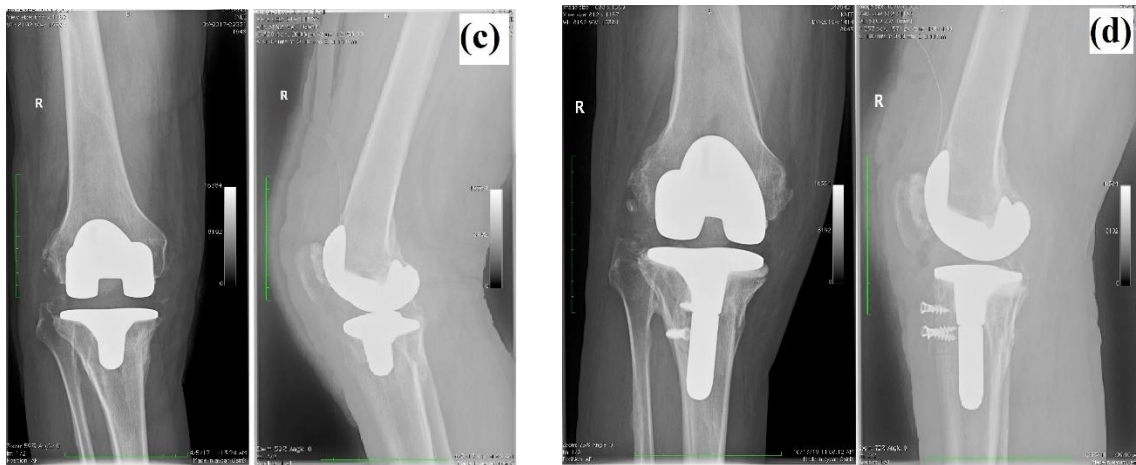
Figure 1. (**a**) Bilateral knee radiography—anteroposterior view, demonstrating advanced degenerative changes (gonarthrosis stadium IV) at the level of the right knee (white arrows), secondary to the malunion of tibial plateau fracture; (**b**) lateral view, showing depression of the lateral tibial plateau (white arrow); (**c**) anteroposterior and later view, eight years after surgery; both views highlight the loosening of the tibial component, minimal osteolysis of the medial tibial plateau (anteroposterior view) and minimal osteolysis around the distal region of the tibial implant (lateral view); (**d**) anteroposterior and lateral view after revision of the total knee arthroplasty using modular tibial implant with short stem and two screws for re-insertion of the patellar tendon (after tibial tuberosity osteotomy).

2.2. Retrieved Components of Knee Prosthesis and confocal Raman Spectroscopy

In Figure 2 are presented the photographic images of retrieved tibial components after 10 years, showing the surface deterioration especially on the surface of UHMWPE component (delamination, scratching), along with the accumulation of pelleted synovial fluid in the stem of tibial component (Figure 2b).
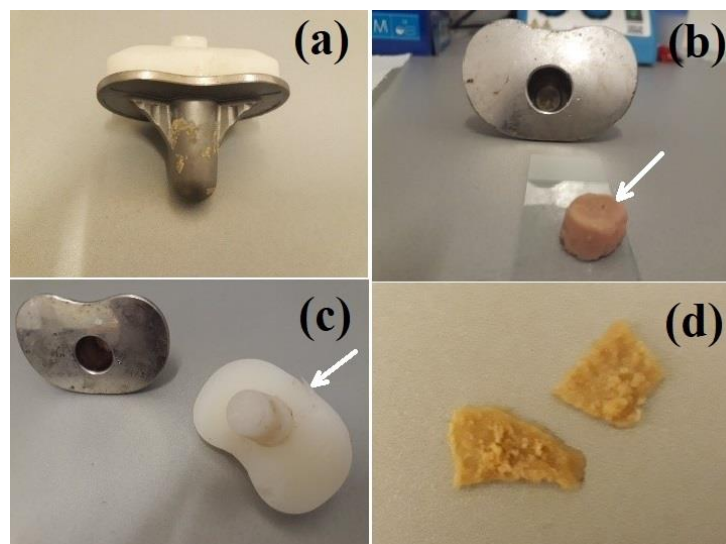
Figure 2. Photographic images of retrieved tibial components of knee prosthesis. (**a**) Assembled tibial components; (**b**) titanium component and synovial fluid collected from the stem (white arrow); (**c**) separate metallic and ultra-high-molecular-weight polyethylene (UHMWPE) component, showing surface delamination (white arrow); (**d**) acrylic cement detached from the metallic component.

Confocal micro-Raman spectra were acquired using an InVia Reflex Raman spectrometer (Renishaw, New Mills, UK) equipped with an upright microscope (Leica). Raman spectra were recorded from the surface of metallic and plastic components using a 785 nm laser diode for excitation. The retrieved plastic and metal were placed under different orientations on the Raman microscope stage to be able to collect distinct Raman signal from exposed surfaces to bone and metal, through a 20× objective (NA 0.35), 30 mW excitation power, 1 accumulation and 1 to 10 s exposure, depending on the collecting mode (short range from 700 to 1800 cm^{-1} or extended mode from 100 to 3200 cm^{-1}). Different data collection modes were applied to control any spectral change associated with longer time exposure to laser of the raw, freshly retrieved biological material. The spectral resolution was $1 cm^{-1}$. The spectral calibration was achieved using an internal silicon standard. The Raman spectral characterization was run to comprise at least 10 spectral acquisitions from different active sites of the knee prosthesis (i.e., the tibial metallic plateau in direct contact with UHMWPE or in contact with biologic tissue, interface between UHMWPE and femoral component, interface between metallic component and acrylic cement, synovial fluid collected from the stem, acrylic cement detached from the tibial component). A total of 159 data files and micrographs were acquired via Raman micro-spectroscopy.

In the case of UHMWPE component, a computational analysis of the relevant spectral regions was applied in the 1000–1200, 1250–1350 and 1400–1500 cm^{-1} intervals respectively. The second-derivative spectra of each interval were smoothed with a nine-point Savitsky–Golay function and the resulted components were used to locate the position of each relevant band component. The curve-fitting analysis was performed by means of Origin 8 software and the spectra were baseline corrected according to the algorithm of Dong et al. [18], assuming a Gaussian profile. The intensity of each spectral band component was further used to calculate the percentage of crystalline (C%) and amorphous (A%) contribution along with the oxidation index (OI) and interpreted in terms of aging influence on the structure of UHMWPE.

The Raman spectra of acrylic cement pieces detached from the metallic tibial component were analyzed in the range 600–3200 cm^{-1} and compared with the abundant literature data on polymethyl methacrylate (PMMA)-based acrylic cement, while the synovial fluid collected from the stem of the tibial component was examined in terms of major Raman bands describing the chemical composition, such as proteins and lipids. Spectra were baseline corrected by multi-point baseline fitting routine and, depending on the comparative purpose, normalized to unit.

3. Results

3.1. Tibial Metallic Component

The micro-Raman spectra and corresponding images recorded on the surface of new (unused) and retrieved tibial component are presented in Figure 3, showing that the spectral features of metallic component (titanium) are well preserved during the implantation interval. Both spectra revealed an intense, broaden band at $144 cm^{-1}$, which is typical for titanium oxide polymorphs [19–22]. Raman scattering is sensitive to material phase and polymorphism. Thus, even though two materials may have identical chemical formulae, any different crystal structure or phase will often result in distinct spectra. According to literature [23] the strongest vibrational mode of anatase polymorph is Eg mode at about $144 cm^{-1}$. The titanium anodization spectra reported by Uttiya et al. [22] using acid media, indicating the formation of titanium oxide layer (crystalline anatase) with typical bands at 144,396,515 and $638 cm^{-1}$. Rutile, other TiO_2 polymorph, exhibits characteristic stretching peaks at 144 (very week), 430 and $590 cm^{-1}$ (very strong) that correspond to the symmetries of B_{1g}, Eg and A_{1g}, respectively. In our case, even if the intense band at $144 cm^{-1}$ may indicate a polymorphism, we noted the absence of all the other Raman active modes of the TiO_2 polymorphs.
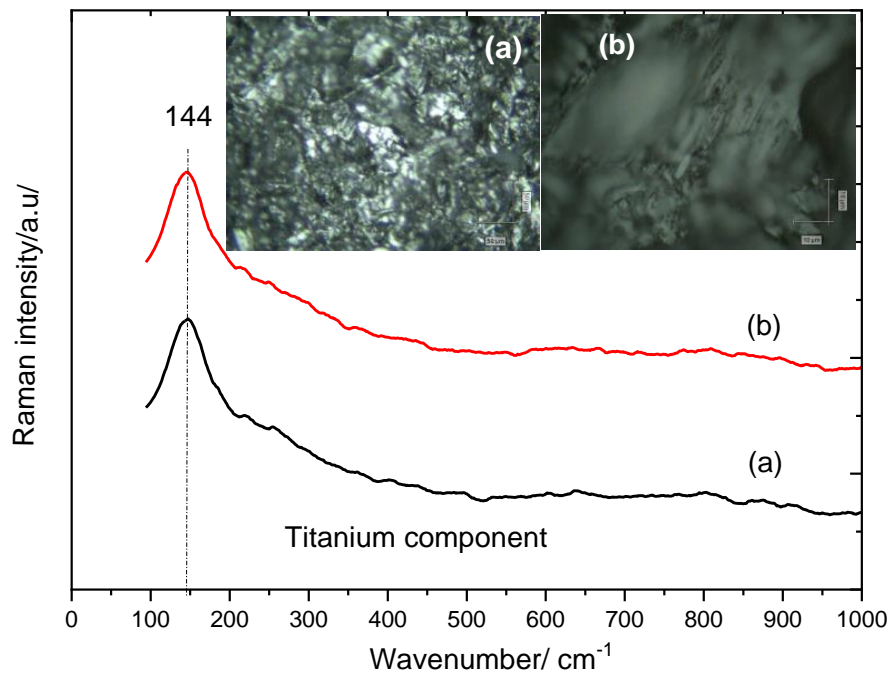
Figure 3. Micro-Raman spectra recorded on the surface of tibial metallic component (titanium). (**a**) As supplied from the producer; (**b**) retrieved prosthetic component along with the corresponding microscopic image (inset). Scale bar 50 μm. Y spectral offset was applied for clarity.

On the other hand, the passive film formation on pure titanium on different anodic potential treatment conditions has been investigated by Zhang et al. [21]. In this case, the overall Raman feature of the oxide layer showed decreased intensity of the Raman modes of anatase and main band (144 cm^{-1}) broadening with decreasing the applied potential. Comparing our result with these reports, we may conclude that our spectra collected from metallic component resembled poor crystalline anatase film on pure titanium, either newly open or after prosthetic retrieval.

Thus, the overall vibrational features (Figure 3) of titanium surface remained unchanged.
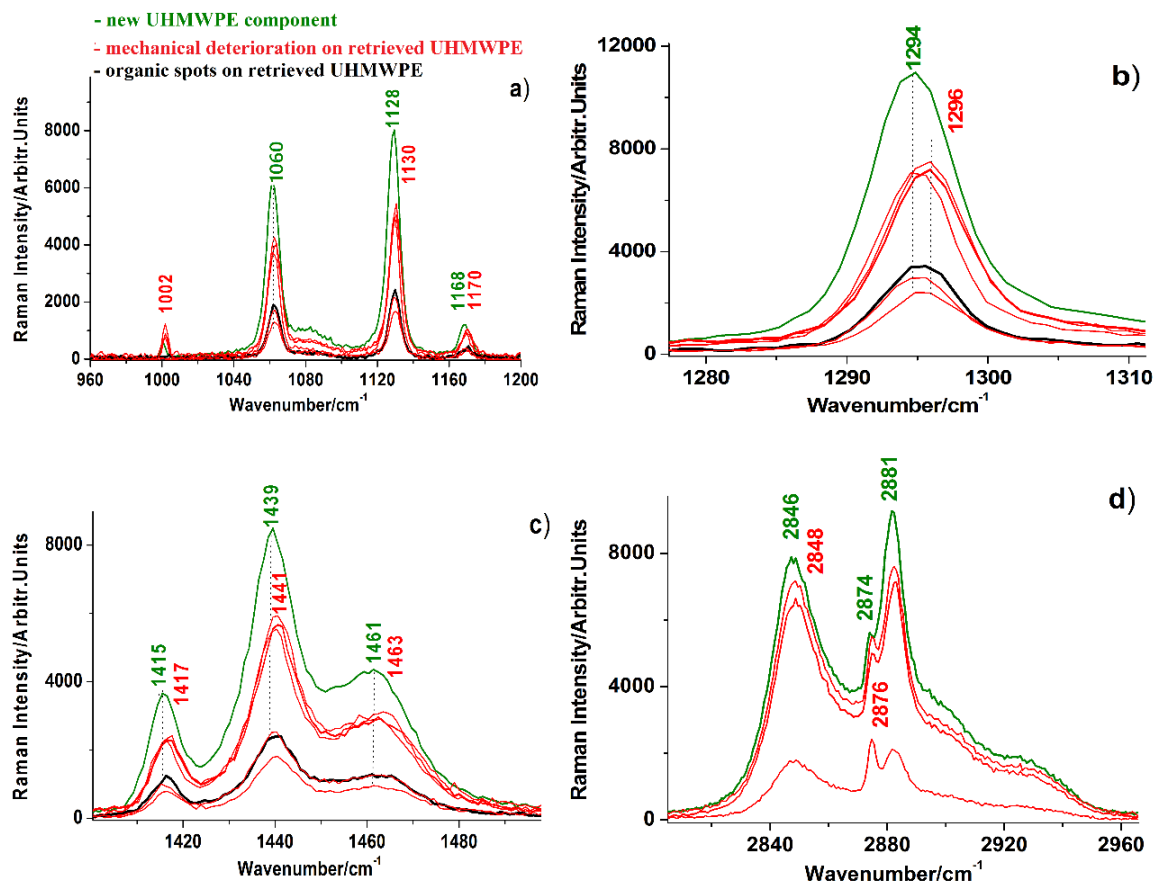
3.2. Aged UHMWPE Component

Multiple Raman spectra were recorded on the surface of UHMWPE component of the retrieved prosthesis and compared with those recorded from a new one (unused, as received from the producer) as presented in Figure 4, highlighting the vibrational details in the main spectral regions. Spectral acquisition was performed from multiple points to comprise the contact interfaces, with the femoral and tibial sites. The corresponding micrographs are presented in Figure 5, showing deterioration signs due to the mechanical contact (scratching and pitting), but also upon interaction with the biologic tissue, as we noticed the presence of persistent organic spots on the surface of retrieved insert. The main vibrational Raman bands are characteristic to polyethylene: 1060, 1128 and 1168 cm^{-1} assigned to the C–C symmetric and asymmetric stretching modes, 1294 cm^{-1} assigned to CH_2 twisting vibrations and the triplet centered at about 1440 cm^{-1} assigned to CH_2 bending modes. In the high wavenumber region, the characteristic peaks of symmetric and asymmetric CH_2, stretching vibration are located at 2846 and 2881 cm^{-1}, respectively [8,24,25].

Comparing the spectra of the new and old plastic, two main characteristics are observed: (i) the systematic slightly shift (2–3 cm^{-1}) toward higher wavenumber in old polyethylene and (ii) a significant decrease of the relative intensities of the main vibrational bands due to aging process.

According to literature [8,24], the most sensitive vibrational bands which involves the structural and morphologic modifications due to oxidation process, and consequently the degree of crystallinity, are 1440, 1294, 1080 and 1310 cm^{-1} band which can be used for the calculation of crystalline and amorphous phase [8,25]. For this purpose, computational analysis by spectral deconvolution and curve fitting procedure was performed for the intervals 1000–1200, 1250–1350 and 1400–1500 cm^{-1}, in order calculate the exact bands intensity, as presented in Figure 6, for both unused and old (retrieved UHMPE) component.

Moreover, since the spectral region between 1250–1350 cm^{-1} is considered to be independent of the polymer chain conformation, the area of the band at 1294 cm^{-1} is accepted as standard to which all the other bands can be related and compared [25].

Figure 4. Micro-Raman spectra acquired from the surface of plastic (UHMWPE) component of a new (green spectra) and retrieved (red) knee prosthesis, showing the vibrational changes (band shifts, relative intensity change) during 10 years aging in human physiological environment. The details of significant intervals are shown in (**a**) 960–1200 cm^{-1}, (**b**) 1280–1310 cm^{-1}, (**c**) 1400–1500 cm^{-1} and (**d**) 2820–2960 cm^{-1} spectral ranges. Spectra acquired under similar excitation and optical collection conditions (excitation: 785, 30 mW, 10 s acquisition, 1 accumulation, 20× objective). Multiple spectra collected from single points of old plastic are shown. Black spectra refer to color spotted plastic supposed to be due to organic micro-deposits, however, the decreased polyethylene signal only was observed.
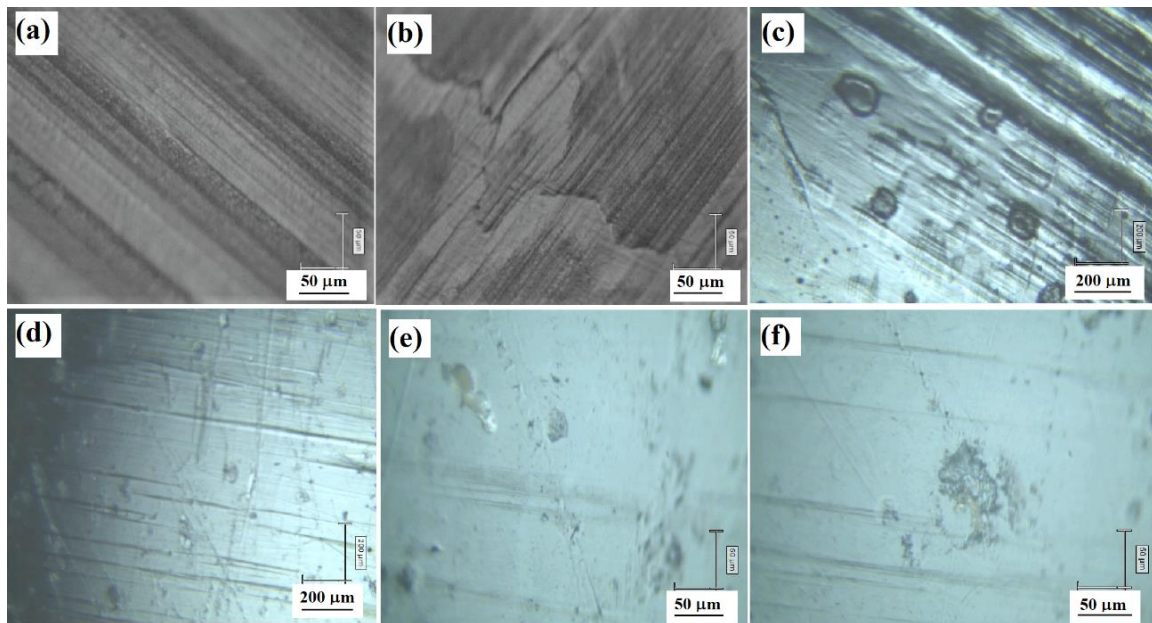
Figure 5. Micrographs recorded in real time on the surface of UHMWPE component during Raman measurements. (**a**,**b**) New (unused) UHMWPE component at the interface with (**a**) tibial and (**b**) femoral sites, respectively; (**c**–**f**) retrieved UHMWPE component—the interface with (**c**) femoral and (**d**) tibial sites, respectively; (**e**,**f**) persistent organic spots detected on the interface.
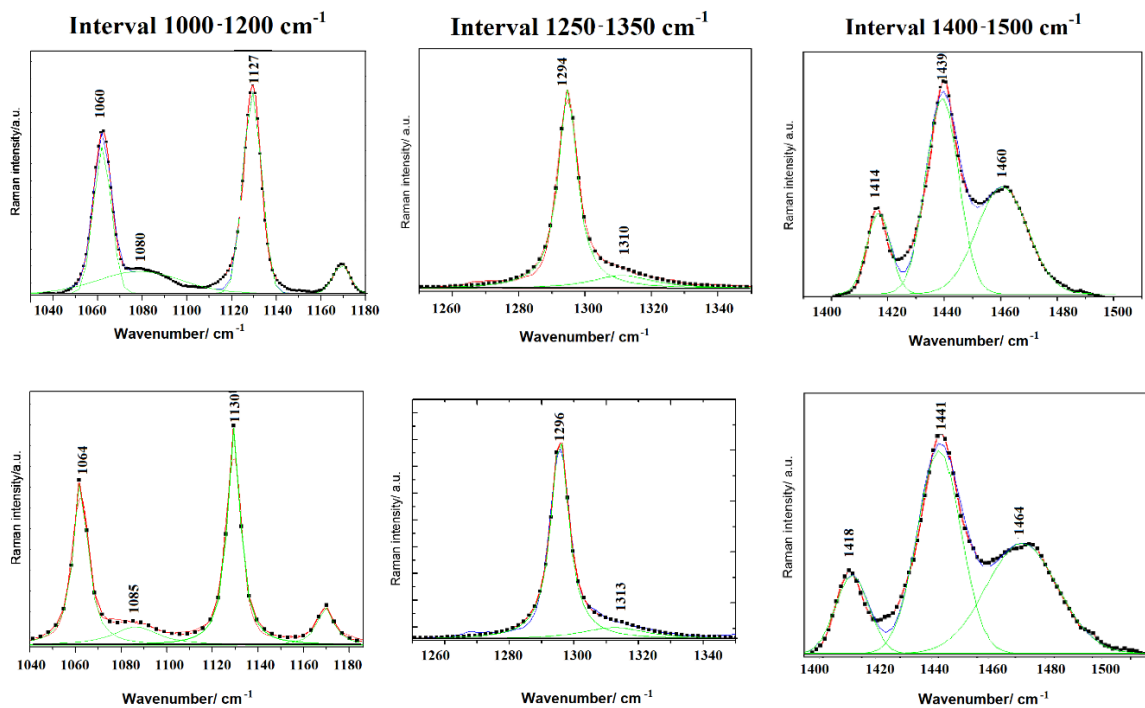
Figure 6. Computational spectral deconvolution and curve fitting procedure of the main wavenumber intervals in Raman spectra and identification of relevant sub-bands: new UHMWPE component (**upper panels**) and retrieved component (**lower panels**).

The values of band intensity determined by spectral deconvolution allows the calculation of crystalline (C%) and amorphous (A%) percentages in each sample along with the oxidation index (OI), according to the following equations [8]:

$$C\% = \frac{I_{1294}}{I_{1294} + I_{1310}} \times 100 \tag{1}$$

$$A\% = \frac{I_{1080}}{0.79(I_{1294} + I_{1310})} \times 100 \tag{2}$$

$$OI = \exp\left\{1.19 \times \tan\left[14.26\left(\frac{I_{1414}}{I_{1294} + I_{1310}} - 0.26)\right] - 0.13\right\} \tag{3}$$

The results of crystallinity, amorphous and oxidation index calculations based on the curve fitting operation of the main Raman bands intensity—for both new and retrieved components—are summarized in Table 1.

Table 1. Values of crystallinity, amorphous and oxidation index calculated according to the Equations (1)–(3) for unused and retrieved polymeric components (main value ± standard deviation).

Parameter	New	Retrieved
C%	46.22 ± 0.2	50.71 ± 0.2
A%	53.52 ± 0.5	48.91 ± 0.3
OI	0.00 ± 0.1	0.37 ± 0.1

It can be noticed an increase of crystallinity degree accompanied by the decrease of amorphous phase in the retrieved component. As the addition of amorphous and crystalline percent does not match the 100%, we can assume the presence of a minor fraction of an intermediate phase [8,26]. On the other hand, a small increase of the oxidation index was noticed in the retrieved component, which is not surprising, as the enhanced crystallinity is often accompanied by the oxidation during in vivo exposure [8,27]. It is considered that a value OI = 3 represent a critical step in the loss of mechanical properties due to fatigue damage in vivo [27,28].

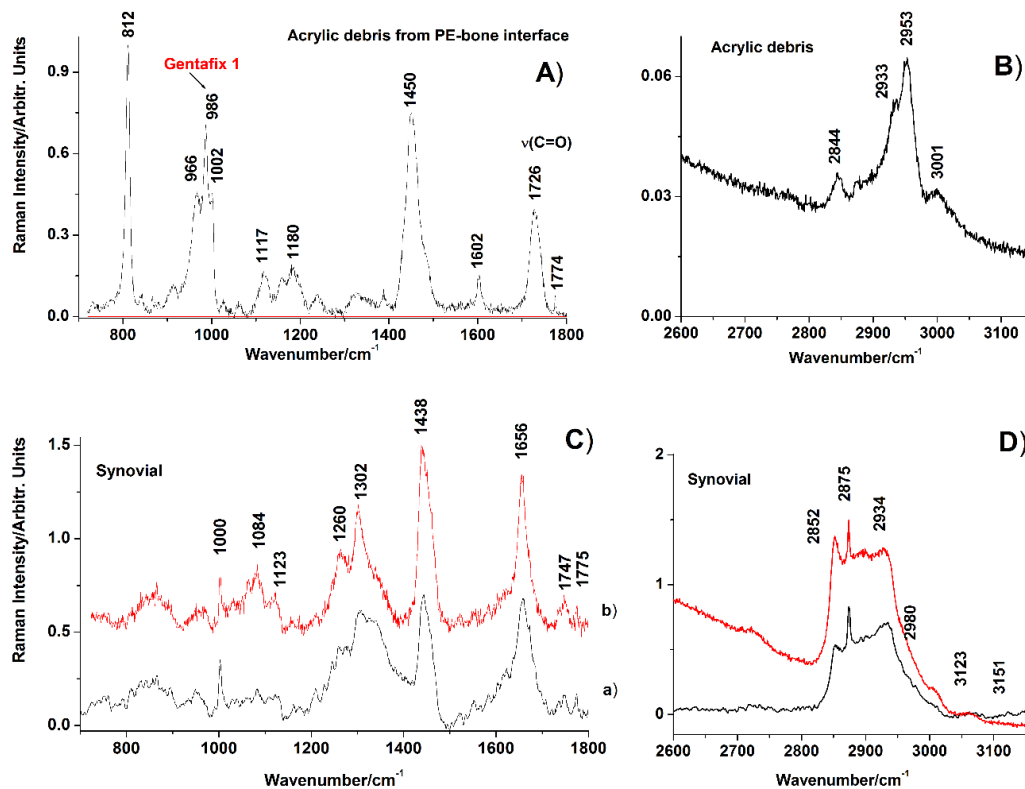### 3.3. Acrylic Cement Debris and Synovial Fluid

The Raman spectra acquired from the surface of acrylic cement detached from the metallic stem is presented in Figure 7A,B in the low and high wavenumber region. The fingerprints of acrylic cement are the strongest band at 2953 cm^{-1}, which is the stretching mode attributable to υ (C–H, CH$_2$, CH$_3$) in PMMA, 1726 cm^{-1}, assigned to υ(C=O) groups stretching mode, 1450 cm^{-1} (strong intensity) due to CH$_3$ and CH$_2$ groups deformation and 812 cm^{-1} (strong and sharp) due to the deformation of C–O–C group. Ten-year-old acrylic cement exhibited several bands that are slightly different from those of pristine PMMA, as shown in Table 2, in comparison with the previous Raman data reported on PMMA [29–31].

The intense band at 986 cm^{-1}, which is absent in pristine-PMMA, represent the signature of gentamicin (C–C stretching vibration) [32], while the characteristic band at 1648 cm^{-1} reported by several authors [29,31] was not observed here. However, this latter band was not reported in the first comprehensive vibrational IR and Raman characterization of PMMA available from Willis et al. [30]. The slight changes in main band positions and occurrence of new band such as that observed at 1602 cm^{-1} which is not observed in synovial fluid either, correlated with the yellow color of the retrieved acrylic cement, may suggest alteration in polymer composition and structural properties.

Table 2. Observed Raman bands/cm^{-1} in aged acrylic cement from prosthetic retrieval compared to literature data of pristine polymethyl methacrylate (PMMA) and their assignment.

PMMA Ref. [29] cm^{-1}	PMMA Ref. [30] cm^{-1}	PMMA Ref. [31] cm^{-1}	Acrylic Cement Debris (This Work) cm^{-1}	Vibrational Assignment [29–31]
833	818, 833	853	812	υ_s(C–O–C) δ (CH$_2$)
			966	Not assigned
995	991 1161 1188 1234	925 999 1081	1002 1117 1180 1234	υ (C–O) ρ (O–CH$_3$) υ_{as}(C–O–C–)
1264	1276	1264		υ (C–O)
1470	1456 1490	1460	1450	υ C–H)
			1602	Not assigned
1645	Not reported	1648	Not observed	υ(C=C) and υ(C–COO)
1739	1736	1736	1726 1774	υ (C=O) of C–OO
	2849 2920	2848	2844 2933	υ(CH$_2$), combination band involving –O–CH$_3$
2952	2957	2957	2953	υ (C–H), CH$_2$, CH$_3$
3001	2995	3001	3001	υ (C–H) of O-CH$_3$ υ (C–H) of –CH$_3$

Abbreviations: υ-stretching, δ-deformation, ρ-rocking.

Figure 7. Micro-Raman spectra collected in the low (**A**) and high wavenumber range (**B**) from the surface of acrylic cement debris detached from the metallic stem, characteristic for acrylic-bone interface; and (**C,D**) synovial fluid spectra from light (a) and dark (b) spotted points, accumulated in the stem of the tibial component. Averaged spectra of 10 distinct points acquisitions are given; spectra were background subtracted and normalized to unit; Excitation: 785 nm, 30 mW.

To assess whether the cement was loaded with synovial components, we comparatively showed its Raman signature (Figure 7C,D) while the corresponding micrographs taken with Raman video camera are showed in Figures 8 and 9.
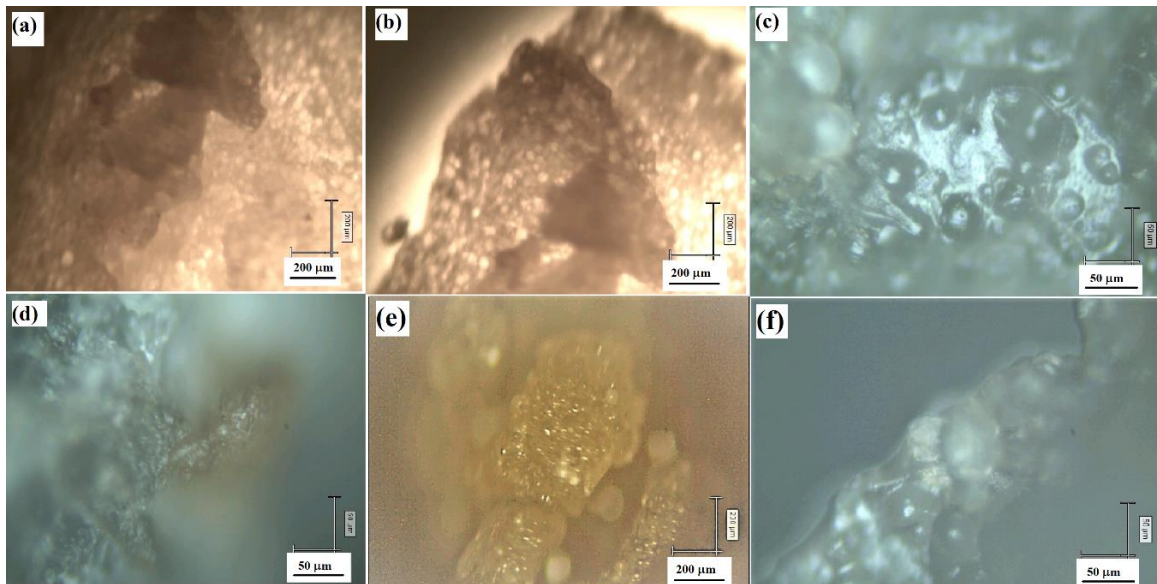
Figure 8. Micrographs corresponding to multiple acquisition performed on different sites of the surface of acrylic cement debris. The images shows details of the acrylic cement surface in contact with the (**a**,**b**) metallic component and with (**c**–**f**) the biologic tissue.
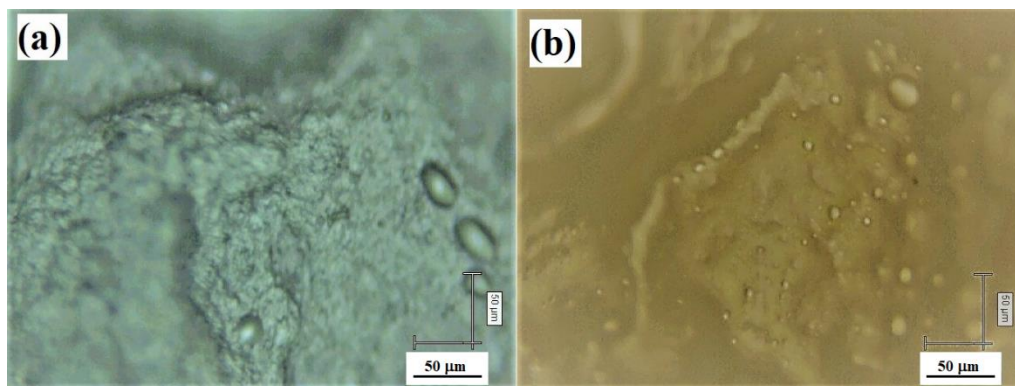
Figure 9. Micrographs corresponding to multiple acquisition performed on different sites on the surface of synovial fluid, showing embedded lipid droplets: (**a**) center, (**b**) edge.

The assignment of vibrational bands related to synovial fluid is summarized in Table 3, based on the literature [33,34].

It is well known that physiological composition of normal synovial fluid includes high level of albumin (6–10 g/L from a total of ~25 g/L proteins), along with γ-globulin and hyaluronic acid [34]. As there are some overlapping of the characteristic vibrational bands of lipids and proteins in the high wavenumber region and also at about 1656 cm^{-1}, we wanted to clarify the main features of synovial fluid by comparing its Raman signature with that of proteins and lipids. As reference spectra, the human serum albumin (HAS, Sigma-Aldrich, St. Louis, MO, USA), collagen from bovine Achilles tendon (Sigma-Aldrich) and vegetal oil (rapeseed) were used from our Raman Lab database as presented in Figure 10. The lipid profile of spectra collected from synovial fluid is evidenced by the intense and sharp band at 2852 cm^{-1} accompanied by broad and weak bands at 2875 and

2934 cm^{-1}, very similar to the spectral features of oils, fat and fatty acids [33]. By comparison, the main Raman feature of albumin and collagen, in the high wave numbers region, is represented by the very intense band at 2930 cm^{-1}. Regarding the assignment of the band at 1656 cm^{-1}, it can be assumed an overlapping of vibrational contribution from proteins and lipids.

Table 3. Assignment of the vibrational bands in Raman spectra of synovial fluid accumulated as pellet deposition in the ten-year-old retrieved prosthetic (Figure 7C,D).

Raman Shift (cm^{-1})	Assignment	Chemical Component
1000	Ring breathing	Proteins, Phe residue
1084	C–C stretching	Fatty acids, triacylglycerols, cholesterol
1123	C–C stretching	Fatty acids, glycerols, cholesterol
1260	=CH deformation	Lipids, fatty acids
1302	CH$_2$ twisting	Fatty acids, cholesterol
1438	CH$_2$/CH$_3$ deformations	Lipids, fatty acids
1656	C=C stretching	Proteins (amide I α-helix), lipids (fatty acids, triacylglycerols)
2852	CH$_2$ symmetric stretching	Lipids, proteins
2875	CH$_2$ symmetric stretching	Lipids, proteins
2934	CH$_3$ asymmetric stretching	Lipids, proteins
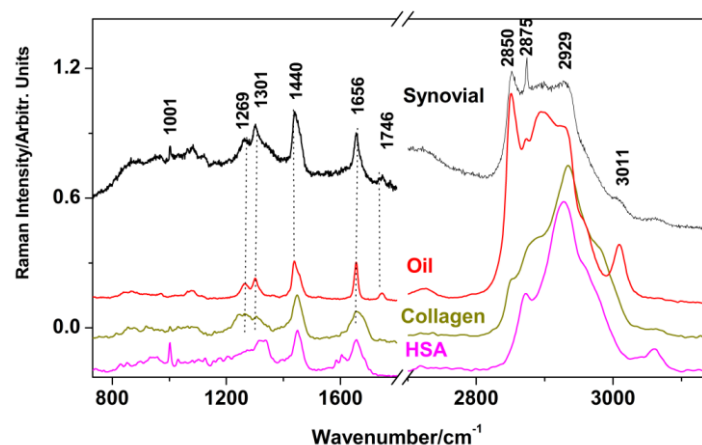
Figure 10. Raw Raman signal of synovial fluid (averaged of 10) compared to the spectra of human serum albumin (HSA) (powder), collagen (powder) and commercial lipid (oil), demonstrating the dominant lipid profile of collected synovial fluid spectrum with proteins signal influence.

4. Discussion

Although the design and surgical fixation techniques in arthroplasty have significantly improved in the last decade, progression of degenerative diseases to the adjacent compartment has commonly been reported as a reason for revision of TKA [7]. The presence of an implant alters alignment and cartilage loading, thus favoring degenerative changes or the production of wear debris (metallic, polymeric, and/or cement). Many clinical evidence as well as retrieval studies evaluated the presence or absence of the damage modes: dishing, embedding, pitting, scratching and extruded cement (cement overhanging the margins of the component), while polyethylene components were also assessed for abrasion, burnishing and delamination [7,10,24,25]. In general, joint simulators allows preclinical evaluation of wear of artificial joints in a controlled environment, the results being similar to those found in retrieved prostheses [7,8]. Specifically, extruded cement may be associated with TKA revision and should be minimized during index surgery. Numerous studies have pinpointed

various factors influencing the extent of wear of the tibial (and patellar) polyethylene components including knee alignment, polyethylene thickness, surface geometry, quality of the polyethylene, manufacturing processes (such as heat treatment of the articular surfaces) and gamma irradiation in air used for sterilizing the components [6,35–37]. From the material point of view, despite the large number of works in recent years that seems to indicate a satisfactory behavior of UHMWPE for bearing applications, further research needs to be carried out in order to properly predict lifetime of these prostheses when implanted.

Vibrational spectroscopy such as FTIR (Fourier Transformed Infrared) and FT Raman are advanced analytical methods, highly precise and nondestructive, fast and very useful in assessing the oxidation range of retrieved UHMWPE components. Oxidized UHMWPE is an inherent state that exists in UHMWPE components used in total joint replacements. The degree of oxidation of UHMWPE components has been linked to changes in the mechanical properties of the material, such as decreased fatigue strength and the production of wear particles around the site of the implant [36,37]. Higher crystalline fraction correspond to a more pronounced oxidative behavior, attributable to the formation of free radicals during in vivo exposure [8,9,35]. Hence, Raman spectroscopy may represent a useful tool on monitoring and controlling the quality of UHMWPE components and would be a feasible choice for investigating the behavior of novel UHMWPE-derived materials with incorporated antioxidant agents like α-tocopherol and others [36].

In our study, confocal Raman spectroscopy was employed for rapid screening of retrieved tibial component of knee prosthesis, evaluating the modifications related to aging process as possible reasons of failure. The metallic tibial component does not show any modification during the implantation period, as demonstrated by the well preserved anatase phase detected in retrieved component, compared to the unused piece.

Generally, metals are subjected to corrosion when in contact with body fluid as the body environment is very aggressive due to the presence of chloride ions and proteins [38]. Specifically, titanium and titanium alloys that come into contact with biologic systems may undergo some degree of corrosion while metal ions released intra-articularly may form complexes with native proteins. These metal–protein complexes may act as antigens or allergens and cause an immunologic response in the body or synovial joint [39]. In this case, we found no evidence of corrosion, and hence, metal ions released cannot be a reason of failure. Evan if the protective and stable oxides on titanium surfaces are able to provide favorable osseointegration, in this case, an oxide-free surface is desired ensuring the best contact with the UHMWPE component. In the retrieved titanium component, the eventually expected oxidation (TiO_2) layer with characteristic Raman bands specific for each polymorph (anatase, rutile, brookite) was not observed [20,22].

To clarify the complex phenomena occurring in vivo in UHMWPE component, accurate structural analyses were performed in the present study, by assessing the crystallinity degree and oxidation behavior of UHMWPE component due to aging process. Polyethylene is a very transparent material to visible lasers, and hence, the penetration depth of the laser can be significant. A careful consideration of the main spectral region was made by comparing a new UHMWPE component with the retrieved one, highlighting important details such as slightly shifts accompanied by reduction of bands intensity due to aging process. Moreover, based on spectral deconvolution and curve fitting procedure, crystalline (C%) and amorphous (A%) percentages in each sample along with the oxidation index (OI) was calculated. An insignificant level of oxidation was demonstrated (OI less than one), while small modifications of crystallinity and amorphous phase were noticed. It is considered that values OI less than one and degrees of crystallinity in the range of 45%–50% does not affect the mechanical properties, but only the wear lifetime with respect to degradation [8,9]. According to previous studies [24], both degrees of crystallinity and amorphous phase were altered by oxidation, but the mechanical strain was considered to be the main factor in alteration of crystallinity. Conversely, the chemical process (oxidation) is the only one affecting the amorphous phase. An interesting study applying Raman confocal spectroscopic technique to quantitatively assess the structural features of two kinds of UHMWPE acetabular cups

belonging to different generations, and thus manufactured by different procedures, demonstrated that oxidation profiles of polyethylene cups belonging to different generations greatly differed after wear testing [8]. In a similar approach, micro-Raman spectroscopy was used to investigate the effects of the sterilization method (gamma and ethylene oxide treatment) on the crystallinity degree of UHMWPE acetabular cups, demonstrating that unworn gamma-sterilized cups were significantly more crystalline than the ethylene oxide-sterilized ones [26]. All these previous works demonstrated the superiority of confocal Raman spectroscopy over other available techniques (such as differential scanning calorimetry or X-rays diffraction) use for quantitative evaluation of polymer crystallinity.

In the present study, the micrographs recorded on the interface of UHMWPE with both metallic component and biologic tissue, evidenced some mechanical damage such as scratches and pitting, along with persistent organic spots. These aspects could be correlated to the decementation observed based on the radiographic examination. PMMA-based acrylic bone cements has been traditionally used for fixation of total joint replacement prostheses to periprosthetic bone, based on radical polymerization of the MMA, which is an exothermic reaction resulting in a temperature increase in the curing bone cement [40]. It has been demonstrated that biodegradation of polymeric bone cements can result from the environment in vivo. For example, acrylic cement specimens retrieved six years after total hip arthroplasty showed significant decrease in fatigue strength compared with unused (control) specimens [41]. On the other hand, some previous works investigating antibiotic release from acrylic bone cements have postulated that water penetrates into the cement through surface cracks and voids, created by the release of gentamicin sulfate [42,43].

The involvement of cement particles in the wear process of knee prosthesis was demonstrated in some previous works [12,44]. For example, Wasielewski et al. [44] reported severe articular and third-body wear from cement debris in a retrieval analysis of 55 polyethylene tibial inserts with deep prismatic scratching of cobalt–chromium alloy condylar components. A more recent study developed in a knee wear simulator, evaluated the influence of third bodies (bone and PMMA-particles) on number, size and shape of wear debris generated [12]. These previous studies demonstrated that free cement debris can significantly increase the generation of wear particles in TKA. Hence, it is basically accepted that particle size, number and morphology will affect the biologic response, resulting in an osteolysis that finally leads to an aseptic loosening in TKA. In our case, the deterioration of acrylic cement due to aging, and third-body wear of cement particles could be a reason of failure, which is also supported by the radiographic examination and the mineralization process evidenced by the Raman spectra of acrylic cement debris. Pre-revision radiographs were evaluated for implant alignment as well as the presence or absence of extruded cement and periprosthetic osteolysis. It is well known that wear is very difficult to assess on conventional X rays, it can appear suddenly before the tenth years after implantation, in the form of early osteolysis, in the case of heavy patients [44–46].

It was previously demonstrated that resonance Raman (RR) and surface-enhanced Raman scattering (SERS) analysis are very useful tools in estimating knee osteoarthritis grading, based on the signature of proteins in synovial fluid [16,17]. An accurate discrimination between low-grade and high-grade osteoarthritis was possible based the molecular changes taking place in the synovial fluid of patients [17]. Moreover, in situ techniques and real time measurements, using epidural needle Raman sensors were recently described, testing the ability of Raman spectroscopy to distinguish each tissue type [47].

In the present work, confocal Raman applied to synovial fluid collected from the stem of the tibial component demonstrated a lipidomic profile, based upon a comparison with commercial lipid sample, human serum albumin and collagen reference samples. According to literature, several clinical studies have revealed correlations between various lipid classes (mainly triglycerides and cholesterols) in serum and synovial fluid with different stage of osteoarthritis, synovitis and wound repair [48]. Hence, in the present case, we may assume that high lipids level could be a cumulative factor involved in failure, complementary to third body wear, which drastically affected the surrounding tissue. By corroborating the clinical and radiological examination with the confocal Raman results, we were

able to evaluate the failure reason of knee implant upon TKA, based on rapid screening of retrieved tibial components.

5. Conclusions

In the present study, a failure situation was investigated upon TKA, in a rapid screening, by combining the clinical evidences with confocal Raman spectroscopy, with high sensitivity and nondestructive measurements. The retrieved components of knee prosthesis (both titanium and UHMWPE component), after 10 years use, were jointly investigated with the assessment of the chemical composition of synovial fluid accumulated in the stem of the tibial component during implantation period. From the material point of view, the metallic component (titanium) did not show any structural modification, as revealed from the Raman spectra. Using confocal micro-Raman spectroscopy, the ten years aged polyethylene showed slight structural changes in terms of Raman signature. Additional changes were noted in the Raman spectroscopy of aged acrylic cement, based on the comparison with the data from pristine PMMA. Metal–plastic aging and the possible scenario of failure due to combined effect of mechanical and biochemical processes that may affect the longevity of knee prostheses are discussed and interpreted in the context of proper functioning and life span of knee prosthesis. The UHMWPE component presents an insignificant level of oxidation (OI < 1), while small modifications of crystallinity and amorphous phase were noticed, as demonstrated by spectral deconvolution and curve fitting procedure. By analyzing the acrylic cement debris and synovial fluid composition we may assume that lipidomic profile and third body wear are cumulative factors of failure in this case. The results are also supported by the clinical and radiographic examination, which evidenced a drastic deterioration of the surrounding tissue. The cement debris affected the biologic response, resulting in an osteolysis and finally an aseptic loosening.

Author Contributions: Conceptualization, C.T.H. and S.C.; methodology, S.C., S.C.P. and A.G.M.; software, S.C. and S.C.P.; validation, S.C.P., S.C. and F.B.; formal analysis, G.M.; investigation, C.T.H., S.C., S.C.P., A.G.M., F.B., G.M.; writing—original draft preparation, S.C., S.C.P. and G.M.; writing—review and editing, C.T.H. and S.C.; supervision, C.T.H. and S.C. All authors have read and agreed to the published version of the manuscript.

References

1.　Wang, J.; Yang, Y.; Guo, D.; Wang, S.; Fu, L.; Li, Y. The effect of patellar tendon release on the characteristics of patellofemoral joint squat movement: A simulation analysis. *Appl. Sci.* **2019**, *9*, 4301. [CrossRef]

2.　Affatato, S.; Valigi, M.C.; Logozzo, S. Wear distribution detection of knee joint prostheses by means of 3D optical scanners. *Materials* **2017**, *10*, 364. [CrossRef] [PubMed]

3.　Nardini, F.; Belvedere, C.; Sancisi, N.; Conconi, M.; Leardini, A.; Durante, S.; Parenti-Castelli, V. An anatomical-based subject-specific model of in-vivo knee joint 3d kinematics from medical imaging. *Appl. Sci.* **2020**, *10*, 2100. [CrossRef]

4.　Bini, S.; Khatod, M.; Cafri, G.; Chen, Y.; Paxton, E.W. Surgeon, implant, and patient variables may explain variability in early revision rates reported for unicompartmental arthroplasty. *J. Bone Jt. Surg. Am.* **2013**, *95*, 2195–2202. [CrossRef] [PubMed]

5.　Fisher, J.; McEwen, H.M.J.; Tipper, J.L.; Galvin, A.L.; Ingram, J.; Kamali, A.; Stone, M.H.; Ingham, E. Wear, debris, and biologic activity of cross-linked polyethylene in the knee: Benefits and potential concerns. *Clin. Orthop. Relat. Res.* **2004**, *428*, 114–119. [CrossRef]

6.　Schwartz, O.; Aunallah, J.; Levitin, M.; Mendes, D.G. Wear pattern of retrieved patellar implants. *Acta Orthop. Belg.* **2002**, *6868*, 362.

7.　Rawal, B.R.; Yadav, A.; Pare, V. Life estimation of knee joint prosthesis by combined effect of fatigue and wear. *Procedia Technol.* **2016**, *2*, 60–67. [CrossRef]

8. Puppulin, L.; Kumakura, T.; Yamamoto, K.; Pezzotti, G. Structural Profile of Ultra-High Molecular Weight Polyethylene in Acetabular Cups Worn on Hip Simulators Characterized by Confocal Raman Spectroscopy. *J. Orthop. Res.* **2011**, *2929*, 893–899. [CrossRef]

9. Kaplan, L.M.; Siljander, M.P.; Verner, J.J.; Baker, K.C.; Gehrke, C.K.; Salisbury, M.R.; Baker, E.A. Analysis of Retrieved Unicompartmental Knee Implants and Tissue: Third-Body Wear as a Potential Contributor to Progression of Arthritis to Adjacent Compartments. *Orthopedics* **2019**, *4242*, 149–157. [CrossRef]

10. Grecu, D.; Antoniac, I.; Trante, O.; Niculescu, M.; Lupescu, O. Failure Analysis of Retrieved Polyethylene Insert in Total Knee Replacement. *Mater. Plast.* **2016**, *5353*, 776–780.

11. Hood, R.W.; Wright, T.M.; Burstein, A.H. Retrieval analysis of total knee prostheses: A method and its application to 48 total condylar prostheses. *J. Biomed. Mater. Res.* **1983**, *17*, 829–842. [CrossRef] [PubMed]

12. Paulus, A.C.; Franke, M.; Kraxenberger, M.; Schröder, C.; Jansson, V.; Utzschneider, S. PMMA third-body wear after unicondylar knee arthroplasty decuples the uhmwpe wear particle generation in vitro. *BioMed. Res. Int.* **2015**, *2015*, 575849. [CrossRef] [PubMed]

13. Landy, M.M.; Walker, P.S. Wear of Ultra-high-molecular-weight Polyethylene Components of 90 Retrieved Knee Prostheses. *J. Arthroplasty* **1988**, *3*, S73–S85. [CrossRef]

14. Mirra, J.M.; Marder, R.A.; Amstutz, H.C. The pathology of failed total joint arthroplasty. *Clin. Orthop.* **1982**, *170*, 175. [CrossRef]

15. Esmonde-White, K.A.; Mandair, G.S.; Raaii, F.; Jacobson, J.A.; Miller, B.S.; Urquhart, A.G.; Roessler, B.J.; Morris, M.D. Raman Spectroscopy of Synovial Fluid as a Tool for Diagnosing Osteoarthritis. *J. Biomed. Opt.* **2009**, *1414*, 034013. [CrossRef]

16. Cinta-Pinzaru, S.; Cavalu, S.; Leopold, N.; Petry, R.; Kiefer, W. Raman and surface-enhanced Raman spectroscopy of tempyo spin labelled ovalbumin. *J. Mol. Struct.* **2001**, *565*, 225–229. [CrossRef]

17. Bocsa, C.D.; Moisoiu, V.; Stefancu, A.; Leopold, L.F.; Leopold, N.; Fodor, D. Knee osteoarthritis grading by resonant Raman and surface-enhanced Raman scattering (SERS) analysis of synovial fluid. *Nanomed. Nanotechnol. Biol. Med.* **2019**, *20*, 102012. [CrossRef]

18. Dong, A.; Caughey, W.S. Infrared methods for study of hemoglobin reactions and structures. *Methods Enzymol.* **1994**, *232*, 139–175.

19. Born, R.; Scharnweber, D.; Rößler, S.; Stölzel, M.; Thieme, M.; Wolf, C.; Worch, H. Surface analysis of titanium based biomaterials. *Fresenius J. Anal. Chem.* **1998**, *361*, 697–700. [CrossRef]

20. Ekoi, E.J.; Gowen, A.; Dorrepaal, R.; Dowling, D.P. Characterization of titanium oxide layers using Raman spectroscopy and optical profilometry: Influence of oxide properties. *Results Phys.* **2019**, *12*, 1574–1585. [CrossRef]

21. Zhang, L.; Duan, Y.; Gao, R.; Yang, J.; Wei, K.; Tang, D.; Fu, T. The effect of potential on surface characteristic and corrosion resistance of anodic oxide film formed on commercial pure titanium at the potentiodynamic-aging mode. *Materials* **2019**, *12*, 370. [CrossRef] [PubMed]

22. Uttiya, S.; Contarino, D.; Prandi, S.; Carnasciali, M.M.; Gemme, G. Anodic oxidation of titanium in sulphuric acid and phosphoric acid electrolytes. *J. Mater. Sci. Nanotechnol.* **2014**, *11*, S106. [CrossRef]

23. Challagulla, S.; Tarafder, K.; Ganesan, R.; Roy, S. Structure sensitive photocatalytic reduction of nitroarenes over TiO2. *Sci. Rep.* **2017**, *7*, 8783. [CrossRef] [PubMed]

24. Kyomoto, M.; Miwa, Y.; Pezzotti, G. Strain in UHMWPE for orthopaedic use studied by Raman micro spectroscopy. *J. Biomater. Sci. Polym. Ed.* **2007**, *18*, 165–178. [CrossRef] [PubMed]

25. Rull, F.; Prieto, A.C.; Casado, J.M.; Sobron, F.; Edwards, H.G.M. Estimation of crystallinity in polyethylene by Raman spectroscopy. *J. Raman Spectrosc.* **1993**, *24*, 545–550. [CrossRef]

26. Taddei, P.; Affatato, S.; Fagnano, C.; Bordini, B.; Tinti, A.; Toni, A. Vibrational spectroscopy of ultra-high molecular weight polyethylene hip prostheses: Influence of the sterilization method on crystallinity and surface oxidation. *J. Mol. Struct.* **2002**, *613*, 121–129. [CrossRef]

27. Puolakka, T.J.S.; Keranen, J.T.; Juhola, K.A.; Pajamäki, K.J.; Halonen, P.J.; Nevalainen, J.K.; Saikko, V.; Lehto, M.U.; Järvinen, M. Increased volumetric wear polyethylene liners with more than 3 years of shelf-time. *Int. Orthoped.* **2003**, *27*, 153–159. [CrossRef]

28. Kurtz, S.M.; Muratoglu, O.K.; Buchanan, F.J.; Currier, B.; Gsell, R.; Shen, F.W.; Yau, S.S. Interlaboratory studies to determine optimal analytical methods for measuring the oxidation the oxidation index of UHMWPE. *Biomaterials* **2001**, *22*, 2875–2881. [CrossRef]

29. Thakur, V.K.; Vennerberg, D.; Madbouly, S.A.; Kessler, M.R. Bio-inspired green surface functionalization of PMMA for multifunctional capacitors. *RSC Adv.* **2014**, *4*, 6677. [CrossRef]

30. Willis, H.; Zichy, V.J.; Hendra, P. The laser-Raman and infra-red spectra of poly (methyl methacrylate). *Polymer* **1969**, *10*, 737–746. [CrossRef]

31. Thomas, K.J.; Sheeba, M.; Nampoori, V.P.N.; Vallabhan, C.P.G.; Radhakrishnan, P. Raman spectra of polymethyl methacrylate optical fibres excited by a 532 nm diode pumped solid state laser. *J. Opt. A Pure Appl. Opt.* **2008**, *10*, 055303. [CrossRef]

32. Zaleski, S.; Clark, K.A.; Smith, M.M.; Eilert, J.Y.; Doty, M.; Van Duyne, R.P. Identification and quantification of intravenous therapy drugs using normal Raman spectroscopy and electrochemical Surface Enhanced Raman Spectroscopy. *Anal. Chem.* **2017**, *89*, 2497–2504. [CrossRef] [PubMed]

33. Czamara, K.; Majzner, K.; Pacia, M.Z.; Kochan, K.; Kaczor, A.; Baranska, M. Raman spectroscopy of lipids: A review. *J. Raman Spectrosc.* **2015**, *46*, 4–20. [CrossRef]

34. Palmieri, B.; Conrozier, T.; Vadalà, M.; Laurino, C. Synoviology: A new chapter entitled to joints care. *Asian J. Med. Sci.* **2017**, *8*, 1–10. [CrossRef]

35. McGloughlin, T.M.; Kavanagh, A.G. Wear of ultra-high molecular weight polyethylene (UHMWPE) in total knee prostheses: A review of key influences. *Proc. Inst. Mech. Eng.* **2000**, *214*, 349–359. [CrossRef]

36. Rocha, M.; Mansur, A.; Mansur, H. Characterization and accelerated ageing of uhmwpe used in orthopedic prosthesis by peroxide. *Materials* **2009**, *2*, 562–576. [CrossRef]

37. MacDonald, D.; Hanzlik, J.; Sharkey, P.; Parvizi, J.; Kurtz, S.M. In vivo oxidation and surface damage in retrieved ethylene oxide-sterilized total knee arthroplasties. *Clin. Orthop. Relat. Res.* **2012**, *470*, 1826–1833. [CrossRef]

38. Sáenz de Viteri, V.; Fuentes, E. Titanium and titanium alloys as biomaterials (Chapter). In *Tribology-Fundamentals and Advancements*; Gegner, J., Ed.; Intechopen: London, UK, 2013. [CrossRef]

39. Lachiewicz, P.F.; Watters, T.S.; Jacobs, J.J. Metal hypersensitivity and total knee arthroplasty. *J. Am. Acad. Orthop. Surg.* **2016**, *2424*, 106–112. [CrossRef]

40. Cavalu, S.; Simon, V. Microstructure and bioactivity of acrylic bone cements for prosthetic surgery. *J. Optoelectron. Adv. Mat.* **2006**, *88*, 1520–1523.

41. Hughes, K.F.; Ries, M.D.; Pruitt, L.A. Structural degradation of acrylic bone cements due to in vivo and simulated aging. *J. Biomed. Mater. Res.* **2003**, *65*, 126–135. [CrossRef]

42. Diez-Pena, E.; Frutos, G.; Frutos, P.; Barrales-Rienda, J.M. Gentamicin sulphate release from a modified commercial acrylic surgical radiopaque bone cement. I. Influence of the gentamicin concentration on the release process mechanism. *Chem. Pharm. Bull.* **2002**, *5050*, 1201–1208. [CrossRef] [PubMed]

43. Ayre, W.N.; Denyer, S.P.; Evans, S.L. Ageing and moisture uptake in polymethyl methacrylate (PMMA) bone cements. *J. Mech. Behav. Biomed. Mater.* **2014**, *3232*, 76–88. [CrossRef] [PubMed]

44. Wasielewski, R.C.; Galante, J.O.; Leighty, R.M.; Natarajan, R.N.; Rosenberg, A.G. Wear patterns on retrieved polyethylene tibial inserts and their relationship to technical considerations during total knee arthroplasty. *Clin. Orthop. Relat. Res.* **1994**, *299*, 31–43. [CrossRef]

45. Massin, P. How does total knee replacement technique influence polyethylene wear? *Orthop. Traumatol. Sur. Res.* **2017**, *103*, S21–S27. [CrossRef] [PubMed]

46. Cavalu, S.; Simon, V. Proteins adsorption to orthopaedic biomaterials: Vibrational spectroscopy evidence. *J. Optoelectron. Adv. Mat.* **2007**, *99*, 3297–3302.

47. Anderson, T.A.; Kang, J.W.; Gubin, T.; Dasari, R.R.; Peter, T.C.; So, P.T.C. Raman spectroscopy differentiates each tissue from the skin to the spinal Cord: A novel method for epidural needle placement? *Anesthesiology* **2016**, *125*, 793–804. [CrossRef]

48. Wu, C.; Kimmerling, K.; Little, D.; Guilak, F. Serum and synovial fluid lipidomic profiles predict obesity-associated osteoarthritis, synovitis, and wound repair. *Sci. Rep.* **2017**, *7*, 44315. [CrossRef]